Journal of Colloid and Interface Science 339 (2009) 208–216

Contents lists available at ScienceDirect

Journal of Colloid and Interface Science

www.elsevier.com/locate/jcis

A modified Cassie–Baxter relationship to explain contact angle hysteresis and anisotropy on non-wetting textured surfaces

Wonjae Choi [a,1], Anish Tuteja [b,1], Joseph M. Mabry [c], Robert E. Cohen [b,*], Gareth H. McKinley [a,*]

[a] Department of Mechanical Engineering, Massachusetts Institute of Technology, Cambridge, MA 02139, United States
[b] Department of Chemical Engineering, Massachusetts Institute of Technology, Cambridge, MA 02139, United States
[c] Air Force Research Laboratory, Propulsion Directorate, Edwards Air Force Base, CA 93524, United States

ARTICLE INFO

Article history:
Received 2 June 2009
Accepted 13 July 2009
Available online 17 July 2009

Keywords:
Cassie–Baxter relation
Contact angle hysteresis
Anisotropic wettability
Roll-off angle
Triple-phase contact line

ABSTRACT

The Cassie–Baxter model is widely used to predict the apparent contact angles obtained on composite (solid–liquid–air) superhydrophobic interfaces. However, the validity of this model has been repeatedly challenged by various research groups because of its inherent inability to predict contact angle hysteresis. In our recent work, we have developed robust omniphobic surfaces which repel a wide range of liquids. An interesting corollary of constructing such surfaces is that it becomes possible to directly image the solid–liquid–air triple-phase contact line on a composite interface, using an electron microscope with non-volatile organic liquids or curable polymers. Here, we fabricate a range of model superoleophobic surfaces with controlled surface topography in order to correlate the details of the local texture with the experimentally observed apparent contact angles. Based on these experiments, in conjunction with numerical simulations, we modify the classical Cassie–Baxter relation to include a local differential texture parameter which enables us to quantitatively predict the apparent advancing and receding contact angles, as well as contact angle hysteresis. This quantitative prediction also allows us to provide an *a priori* estimation of roll-off angles for a given textured substrate. Using this understanding we design model substrates that display extremely small or extremely large roll-off angles, as well as surfaces that demonstrate direction-dependent wettability, through a systematic control of surface topography and connectivity.

© 2009 Elsevier Inc. All rights reserved.

1. Introduction

When a liquid droplet contacts a flat homogeneous solid surface the droplet establishes a uniquely defined equilibrium contact angle θ_E on the surface which is described by Young's relation [1]. On the other hand, when the same droplet is placed in contact with a rough surface possessing the appropriate combination of surface texture and solid surface energy, the liquid may not penetrate fully into the surface texture, but rather 'bead-up' to form a composite (solid–liquid–air) interface, as shown in Fig. 1a [2–4]. The formation of a composite interface typically enhances the liquid-repellency of the surface, as the liquid droplet sits partially on air (see Fig. 1b).

Cassie and Baxter made the first attempts to correlate the measured apparent contact angles for a composite interface with the details of the solid surface texture [2], based on an implicit assumption [5] that upon the formation of a composite interface, a given liquid droplet reaches a uniquely defined apparent 'equilibrium' contact angle θ_E^* to minimize the overall free energy of the system as it does on flat surfaces. Provided the feature size of the surface texture is much smaller than the size of the liquid droplet, the free energy of the system reaches the global minimum when the apparent contact angle θ_E^* of the composite interface attains a value described by the Cassie–Baxter (CB) relation [2,4,5],

$$\cos\theta_E^* = r_\phi \phi_s \cos\theta_1 + (1-\phi_S)\cos\theta_2 \tag{1}$$

where ϕ_s is the areal fraction of the liquid–air interface occluded by the texture (marked as black in Fig. 1c) and r_ϕ is the 'roughness' of the wetted surface (i.e., the ratio of the actual surface in contact with the liquid to the projected area of the wetted region). The quantities $r_\phi\phi_s$ and $1-\phi_s$ are the areal ratios of the solid–liquid interface (A_{sl}; marked as green in Fig. 1c) and the liquid–air interface (A_{lv}; marked as gray), respectively, compared to the total projected area (A_{total}) of the composite interface. Finally, θ_1 and θ_2

Abbreviations: CB, Cassie–Baxter; CAH, contact angle hysteresis; TCL, triple-phase contact line.

* Corresponding authors. Fax: +1 617 258 8559 (G.H.M.), +1 617 258 8224 (R.E.C.).
E-mail addresses: recohen@mit.edu (R.E. Cohen), gareth@mit.edu (G.H. McKinley).

[1] These authors contributed equally to this work.

0021-9797/$ - see front matter © 2009 Elsevier Inc. All rights reserved.
doi:10.1016/j.jcis.2009.07.027

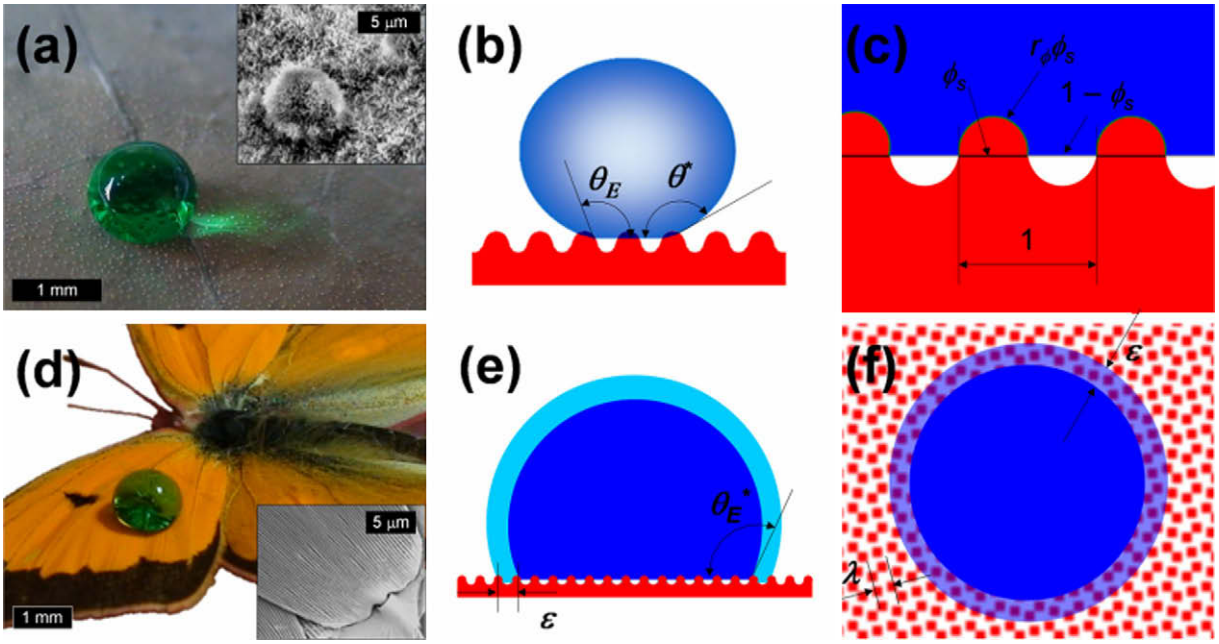

Fig. 1. The correlation between the details of the surface texture and the behavior of the contacting liquids. (a) A droplet of water (colored green), beading up on a superhydrophobic lotus leaf. The inset shows an SEM image of the lotus leaf, highlighting the multiple scales of roughness present on the leaf's surface. (b) A schematic drawing illustrating the formation of a composite interface. (c) A schematic diagram illustrating the various characteristic geometrical parameters used in the Cassie–Baxter relation. (d) A droplet of water on the wings of a butterfly (*Colias fieldi*, also known as pinkedged sulphur). The inset shows an SEM micrograph of the wing, and highlights its stripe-shaped surface texture. The water droplet remains pinned on the surface leading to a significant roll-off angle $\omega > 10^\circ$ when advancing and receding across the striped texture. (e) A schematic diagram illustrating the small displacement of the TCL (ε). (f) Top view for a droplet as the TCL is displaced from its original position by a distance ε, which is on the same order as the characteristic pitch for a given surface texture (λ).

refer to the equilibrium contact angles on solid (=θ_E) and air (=180°) phases, respectively [4,6].

The CB relation is widely used [7]; however, there has been a long-standing debate in the literature regarding the range of applicability, as well as the accuracy of the CB relationship [5,7–19]. This dispute stems from the fact that a range of contact angles θ^* can be established on a given composite interface as a droplet advances or recedes. The contact angle hysteresis (CAH; $\Delta\theta^* = \theta^*_{adv} - \theta^*_{rec}$) is the difference between the apparent advancing and receding contact angles, and is a measure of the 'stickiness' of a surface, i.e., the resistance to motion, experienced by a droplet as it rolls off a surface [20–22]. Indeed, many natural superhydrophobic surfaces utilize CAH to control the behavior of the contacting water droplets, e.g., negligible roll-off angles on Lotus leaves [23], directional wettability on stripe-textured butterfly wings (see Fig. 1d) [14], or sticky composite interfaces on rose petals [24]. However, the CB relation predicts only a single value of the apparent contact angle θ^*_E, and consequently, the relation is inherently unable to provide an explanation for these observations of CAH. Indeed, numerous groups have noted the inability of the CB relation to predict apparent advancing and receding contact angles on a range of textures [7,8,10,11,13–15,25]. These issues have been highlighted recently by Gao and McCarthy, who challenged the validity of the CB model by demonstrating significant differences between the CB predictions and their experimental measurements of the apparent contact angles on heterogeneous surfaces [7]. Several studies [16–18] have attempted to reconcile the experimental observations of Gao and McCarthy with the CB relation by suggesting that the CB relation is valid as long as one considers the local values of the areal fractions of the solid–liquid ($r_\phi\phi_s$) and liquid–air ($1-\phi_s$) interfaces in the vicinity of the triple-phase contact line (denoted TCL for brevity). They pointed out that this local areal fraction can be very different from the global fraction for surfaces with spatially varying patterns. The local wetted fraction was obtained using differential solid–liquid and liquid–air interfacial areas, assuming a displacement of the TCL (denoted ε in Fig. 1e and f) over one full period of surface texture (λ in Fig. 1f). Using the concept of local areal fraction, they demonstrated that the apparent contact angle can vary significantly depending on the specific position of the TCL for surfaces. However, most of these studies did not address the issue of the observed CAH on natural and synthetic surfaces, and were again challenged by Gao and McCarthy [25].

Through the years, various groups have tried to modify the classical CB relation in order to enable it to predict the apparent advancing and receding angles, and thereby, contact angle hysteresis. The different modifications can be broadly classified into two categories, based on the inherent assumptions used to correlate the details of the surface texture with the resulting apparent contact angles; (i) The observed apparent contact angles deviate from the predictions of the CB model due to distortion of the TCL [8,9,25,26]. (ii) The contact angles are determined by the linear fractions of solid and air calculated along the TCL, not by the overall areal fractions [5,7,10,27–29]. However, most of these studies, with the noteworthy exception of the work of Extrand [10], did not quantitatively compare their predictions with experimental values, or reported only contact angles on prototypical textured geometries. Furthermore, many of the studies in category (ii) did not actually compute the apparent contact angles because the linear fractions of the solid and air are extremely hard to predict due to the contorted nature of the TCL on heterogeneous surfaces. To overcome this limitation, certain studies have assumed the existence of an undistorted TCL [10,28,29], which strongly contradicts the fundamental assumption made by groups in category (i) above.

The resolution of this dispute requires experimental enquiry at two distinct length scales: imaging the local distortion of the TCL on the micron scale, as well as measuring the apparent contact angles of macroscopic (i.e., millimeter-sized) liquid droplets on a

composite interface. Scanning electron microscopy (SEM) is an extremely versatile technique for imaging microscopic liquid condensation [30,31]; however, the direct imaging of the TCL of a macroscopic droplet forming a composite interface on a textured surface using an SEM has so far been very rare [32], because many liquids, including water, easily vaporize at the extremely low pressures present inside an SEM chamber. A potential alternative is to use non-volatile organic liquids such as dibenzyl ether or droplets of a curable polymer [33]; however, the imaging of a non-wetting droplet requires that the textured surface be able to support a composite interface with relatively-low surface tension organic liquids. In our recent work, omniphobic textured surfaces were created with re-entrant topographical features that are able to support a composite interface even with liquids possessing extremely low surface tensions, such as methanol and pentane [6,34,35]. In the present study we fabricate a range of micro-hoodoo surfaces ([34]; also see Supplementary material) that support a robust composite interface with a curable polymer polydimethylsiloxane (PDMS).

To inspect the details of the TCL, we deposited droplets of uncured PDMS (γ_{lv} = 19.8 mN/m, θ_E = 68°, droplet volume: 30 – 50 μl) on a number of hoodoo surfaces that had previously been dip-coated with low surface energy fluorinated molecules (fluoro-POSS; [34,36]) to allow higher equilibrium contact angles θ_E [37]. The PDMS drops were then thermally cured. The long equilibration time of the uncured PDMS droplets, resulting from their high viscosity (μ = 5500 mPa·s), makes them unsuitable for contact angle measurements using a contact angle goniometer. Therefore, another organic liquid, decane (γ_{lv} = 23.8 mN/m, θ_E = 70° on a fluoro-POSS dip-coated smooth silicon wafer) was chosen for the contact angle measurements because it possesses a surface tension and equilibrium contact angle that are similar to the values of the PDMS oil used in our imaging.

2. Materials and methods

2.1. Fabrication and dip coating process of micro-hoodoo surfaces

Four inch test grade *p*-type silicon wafers were purchased from Wafernet, Inc. A 300 nm thick silicon dioxide thin film was first deposited on piranha-cleaned silicon wafer, by PECVD. Cap geometries were defined via standard photolithography using OCG825 as the photoresist. Cap patterns were then transferred onto silicon dioxide using a CF_4 plasma RIE. Etch depth was set to 400 nm to expose the bare silicon surface. The caps were then released with severe re-entrance using vapor-phase XeF_2 isotropic etching. Finally, the surface was cleaned with piranha solution (1:3 mixture of H_2SO_4 and H_2O_2). The height of the supporting pillars and the cap thickness were held fixed at 7 μm and 300 nm, respectively. After the fabrication, the samples were immersed in a solution of fluorodecyl POSS in Asahiklin – AK225 (concentration of 3 wt.%). The samples remained in solution for 5 min, after which they were removed and dried in an oven at 60 °C for 30 min. The types of fabricated micro-hoodoos include anisotropic stripe-textured, discrete, inverse, concentric ring-textured, and spiral micro-hoodoos. Detailed dimensions of each of the fabricated micro-hoodoo surfaces are included in the Supplementary material.

2.2. SEM imaging of PDMS droplet

Sylgard® 184 silicone elastomer kit was purchased from Dow Corning, Inc. The mixing ratio of the PDMS and the crosslinker was 10:1. A PDMS droplet with a typical size of 30–50 μl was deposited on each of the various dip-coated micro-hoodoo surfaces, which were tilted by 10–30° to force the PDMS droplet to advance or recede along the inclined hoodoo surface. The droplet was then thermally cured in an oven at 85 °C for 30 min. There is negligible change (<1°) in the value of the equilibrium contact angle θ_E of a PDMS droplet before and after annealing.

2.3. Contact angle measurement

The contact angles for decane were measured using a contact angle goniometer, VCA2000 (AST Inc.). The advancing contact angle was measured by advancing a small volume of decane droplet (typically 5 μl) onto the surface, using a syringe. The receding contact angle was measured by slowly removing the liquid from a drop already on the surface. For each sample a minimum of four different readings were recorded. Typical error in measurements was ~2°.

3. Results and discussion

A surface micro-texture that is well-known to deviate from the CB relation is the stripe texture [8,38,39], which is a synthetic counterpart of a butterfly wing [14] or a rice leaf [40]. Fig. 2 shows an SEM micrograph of a cured PDMS droplet supported on a micro-hoodoo surface possessing a stripe texture (the hoodoo width and

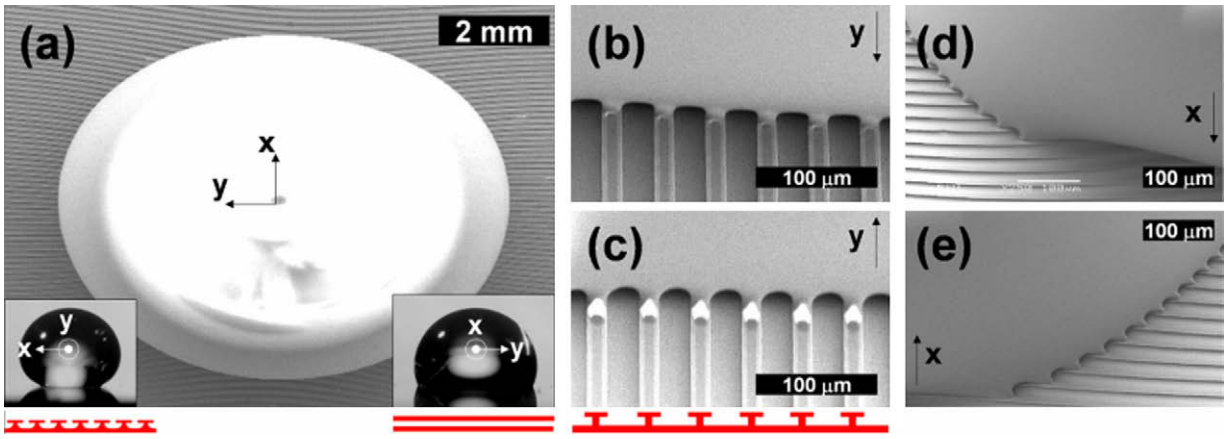

Fig. 2. Details of the advancing and receding TCL for a PDMS droplet on a stripe-textured hoodoo surface. (a) Top view of a droplet of PDMS, deposited and cured on a stripe-textured micro-hoodoo surface (ϕ_s = 0.44). Charge accumulation on the large PDMS drop from the electron beam results in the local lensing and distortion of the hoodoo stripes at the top of the image. The insets show side views of a droplet of decane (θ_E = 70°), viewed along the *y*-axis (left) and the *x*-axis (right). (b) The details of the TCL as the PDMS droplet advances along the *y*-axis. (c) The details of the TCL as the PDMS droplet recedes along the *y*-axis. (d) The details of the TCL as the PDMS droplet advances along the *x*-axis. (e) The details of the TCL as the PDMS droplet recedes along the *x*-axis.

interspacing were 17.6 μm and 22.4 μm, respectively, yielding $\phi_s = 0.44$; note that the thin, flat, and highly re-entrant caps employed in this work allow the simplification of Eq. (1) by using $r_\phi \approx 1$; see Supplementary material for detailed characteristics of the fabricated hoodoo surfaces). Because the dimensions of the hoodoo surface texture are much smaller than the PDMS droplet, the CB relation yields a unique value of the apparent contact angle and the droplet is predicted to be essentially a spherical cap. In contrast, Fig. 2a shows that the PDMS droplet is significantly distorted into an ellipse. The anisotropy is further illustrated by the different values of the apparent contact angles measured along the *x* and *y* directions for a decane droplet (see insets of Fig. 2a). The measured values of the apparent contact angles for decane advancing or receding along the surface in the *y* direction (when the TCL moves along the stripes; see Fig. 2b and c), are $\theta^*_{adv,y} = 119^\circ$ and $\theta^*_{rec,y} = 110^\circ$. These measurements are very close to the predictions of the CB relation ($\theta^*_E = 114^\circ$; using $\theta_1 = 70^\circ$, $\theta_2 = 180^\circ$, $r_\phi = 1$, and $\phi_s = 0.44$ in Eq. (1)). However, if we measure the apparent contact angles along the *x* direction (i.e., the TCL moves across the stripes), we obtain apparent advancing and receding angles of $\theta^*_{adv,x} = 165^\circ$ and $\theta^*_{rec,x} = 107^\circ$, even though the values of r_ϕ and ϕ_s in Eq. (1) are unchanged. These values of the measured contact angle are far from those predicted by the CB relation and cause substantially increased CAH. Indeed, even though the mathematical formula developed by Cassie and Baxter does not account for this anisotropy, Cassie and Baxter warned about this anisotropic wettability by noting "The present analysis is inapplicable when the wires are parallel to the surface" in their original paper [2]. Such directional hysteresis is utilized by various natural surfaces to guide the movement of contacting water droplets along a particular axis [14,40].

3.1. A differential parameter for a modified Cassie–Baxter relation

To provide accurate predictions of the apparent advancing and receding contact angles on textured substrates, we modify the classical CB relation by introducing a new surface texture parameter ϕ_d, where the subscript *d* is used because the parameter is calculated using 'differentially small' solid and air regions during a hypothetical displacement of the TCL ($\varepsilon \ll \lambda$ in Fig. 1e and f). The idea of using a derivative of the droplet free energy with respect to the position of the TCL was proposed by Johnson and Dettre, to predict the advancing and receding angles on a surface patterned with chemically heterogeneous concentric rings [5]. For isotropically textured surfaces (i.e., surfaces whose texture is everywhere similar [16]), the global free energy minimum is always attained at the apparent contact angle θ^*_E given by the classic CB relation. However, many other apparent contact angles can be locally metastable if the system is trapped inside a local free energy minimum [5]. The change in free energy should be calculated for an infinitesimally small hypothetical displacement of the TCL (so that ε in Fig. 1e and f is much smaller than the topographical feature size λ or $(\varepsilon/\lambda) \to 0$), which allows the definition of the differential parameter ϕ_d, so that $r_\phi\phi_d = (\delta A_{sl}/\delta A_{total})_{(\varepsilon/\lambda)\to 0}$ and $1 - \phi_d = (\delta A_{lv}/\delta A_{total})_{(\varepsilon/\lambda)\to 0}$. These definitions more accurately reflect the *differential areas* of the solid–liquid (δA_{sl}) and liquid–air (δA_{lv}) interfaces (compared to the total differential area δA_{total}) that are *traversed* by the TCL during the translation ε. As noted previously, it was theoretically demonstrated that the difference between the differential parameter ϕ_d and the global measure ϕ_s disappears at large displacements of the TCL, i.e., when $\varepsilon \gg \lambda$ [16,18] on isotropically textured surfaces. However, in case of infinitesimal displacements the values of ϕ_d may deviate considerably from ϕ_s. Thus, the local criterion for a minimum in the free energy can be satisfied by the apparent contact angle given by the relation

$$\cos\theta^* = r_\phi\phi_d\cos\theta_1 + (1-\phi_d)\cos\theta_2 \tag{2}$$

Note that ϕ_d remains an areal ratio, which can be simplified to the previously proposed [10,28] linear fractions only under certain limiting cases (see Supplementary material). The concept of the differential area parameter is especially useful when the TCL is located on the boundary between heterogeneous regions, a boundary for which neither linear fraction nor local areal fraction can be uniquely defined. Furthermore, even for the same location, there can be two values of the differential parameter depending on whether the TCL is advancing or receding. It should, however, be noted that the differential parameter defined in the present work can be accurately calculated only when the direction of the TCL displacement can be anticipated.

The apparent advancing contact angle θ^*_{adv} is the maximum contact angle that is locally stable in the microscopic proximity (i.e., at distances less than λ) of the original TCL location. It is clear from Eq. (2) that, provided $\cos\theta_1 > \cos\theta_2$, this angle is maximized at the lowest value of the ratio $r_\phi\phi_d/(1-\phi_d)$. Assuming the roughness of the wetted solid–liquid interface r_ϕ is spatially homogeneous, $r_\phi\phi_d/(1-\phi_d)$ is minimized when the differential parameter ϕ_d reaches its minimum or $\phi_{d,adv} = \min\phi_d|^{\lambda}_{-\lambda}$. The apparent receding contact angle observed as liquid is gradually removed from the drop is defined in an analogous way, thus $\phi_{d,rec} = \max\phi_d|^{\lambda}_{-\lambda}$. As a result, the apparent advancing and receding contact angles should be predicted by the modification of the CB relation proposed below:

$$\cos\theta^*_{adv} = r_\phi\phi_{d,adv}\cos\theta_1 + (1-\phi_{d,adv})\cos\theta_2 \tag{3a}$$

$$\cos\theta^*_{rec} = r_\phi\phi_{d,rec}\cos\theta_1 + (1-\phi_{d,rec})\cos\theta_2 \tag{3b}$$

Figs. 2b and c illustrate details of the distorted TCL for a PDMS droplet on the stripe-textured hoodoos, as the droplet advances (Fig. 2b) or recedes (Fig. 2c) in the *y* direction. The local distortion of the TCL is maximized along the *y* direction, because PDMS forms an equilibrium angle θ_E (≈68°) on the dip-coated silicon substrate and 180° on air. However, there is no change in the differential parameter ϕ_d along the stripes, thus $\phi_{d,adv} = \phi_{d,rec} = \phi_s$ (see Supplementary material for the details). This is the reason for the close match between the measured advancing or receding contact angles along the *y* direction and the apparent contact angle predicted by Eq. (1). The other important observation is that both the apparent advancing and receding contact angles match the prediction from the CB relation despite the severe distortion of the TCL. This result clearly demonstrates that the distortion of the TCL [9,25] *per se* is not the factor that leads to significant difference between predictions from the CB relationship and the measured apparent contact angles.

Fig. 2d shows the local structure of the TCL for a PDMS droplet advancing across the stripes in the *x* direction. As previously noted, a significant discrepancy between the apparent advancing angle with decane ($\theta^*_{adv,x} = 165^\circ$) and the prediction from the CB relation ($\theta^*_E = 114^\circ$) was measured. It is clear from the figure that the advancing front of the TCL at the leading edge of the drop is almost straight and parallel to the striped hoodoo texture, offering additional evidence that the deviation of the apparent contact angles from the CB prediction is not simply a direct consequence of the distortion of the TCL. In this case, the additional local area that is covered by an incremental advancement of the TCL in the *x* direction, from the outer edge of one hoodoo to the next hoodoo, is composed only of air. Thus, $\phi_{d,adv} = 0$ and the TCL remains energetically pinned at the outer edge of the hoodoos until the apparent angle reaches the advancing apparent angle $\theta^*_{adv,x} \to 180^\circ$. The measured value of $\theta^*_{adv,x} = 165^\circ$ is close to, but not exactly same as the prediction. This is because vibrational perturbations from the laboratory environment always provide extra energy input which allows the droplet to relax at least partially [5].

On the other hand, as the drop attempts to recede along the x direction, the TCL becomes pinned on a given hoodoo stripe because of the locally high differential parameter $\phi_{d,rec} = 1$. As liquid is removed, the apparent contact angle here decreases until it eventually reaches the receding angle of the TCL in the y direction (along the stripes), which is determined by the differential parameter along the y direction ($\phi_{d,rec} = 0.44$). As the TCL in the x direction is still pinned, but is free to move along the y direction, the droplet perimeter becomes increasingly circular until the TCL can finally recede along the x direction by suddenly retracting from one hoodoo stripe (in the x direction), following which the droplet becomes anisotropic once more. Hence, in this case, $\phi_{d,rec,x} = \phi_{d,rec,y} = \phi_s = 0.44$, and it may be anticipated that $\theta^*_{rec,x} \approx \theta^*_{rec,y} \approx \theta^*_E$, as was experimentally observed.

The difference between the local TCL movements as the liquid advances or recedes across the hoodoos is further demonstrated using simulations based on the Surface Evolver finite element method ([41]; see Supplementary material). It is clear from our simulations that the advancing TCL remains pinned at the edges of the hoodoos, while the receding TCL can easily recede across the stripes.

We also study apparent contact angles on discrete hoodoo surfaces which are synthetically analogous to natural surfaces such as lotus leaves [23] or rose petals [24]. Although both of these natural surfaces resist wetting by water through the formation of a composite interface, the CAH observed on rose petals is significantly higher than the values observed on lotus leaves [24]. Fig. 3a and b shows the advancing and receding TCL for a PDMS droplet on a micro-fabricated discrete hoodoo surface ($\phi_s = 0.44$). For such a surface, $\phi_{d,adv} = 0$ and $\phi_{d,rec} = \sqrt{\phi_s} = 0.67$ (see Table 1; also see Supplementary material for derivation). Using these values, Eq. (3) predicts $\theta^*_{adv} = 180^\circ, \theta^*_{rec} = 96^\circ$ for a decane droplet on the hoodoo surface. Similarly, numerical analysis using Surface Evolver [41] gives $\theta^*_{adv} = 180^\circ, \theta^*_{rec} = 99^\circ$ (see Fig. 3c and d). These results are in good agreement with the measured apparent contact angles of $\theta^*_{adv} = 164^\circ, \theta^*_{rec} = 100^\circ$. In comparison, the apparent contact angle predicted by the classic CB relation is $\theta^*_E = 114^\circ$.

We can also use Eq. (3) to understand the reason for the significantly different hysteretic behavior of the lotus leaf, compared to the rose petal. The submicron-length scale wax tubules on the nubs of the lotus leaf lead to a composite interface with a very low fraction of the water-wetted solid surface, i.e., $r_\phi \phi_s \to 0$ [23]. This low global areal solid fraction results in an insignificant difference between $\phi_{d,adv}$ (=0) and $\phi_{d,rec} (= \sqrt{\phi_s})$ and correspondingly negligible CAH. On the other hand, the composite interface formed on the rose petal has a significantly higher value of $r_\phi \phi_s$ [24], and this leads to a substantial difference between $\phi_{d,adv}$ and $\phi_{d,rec}$ and, therefore a large CAH.

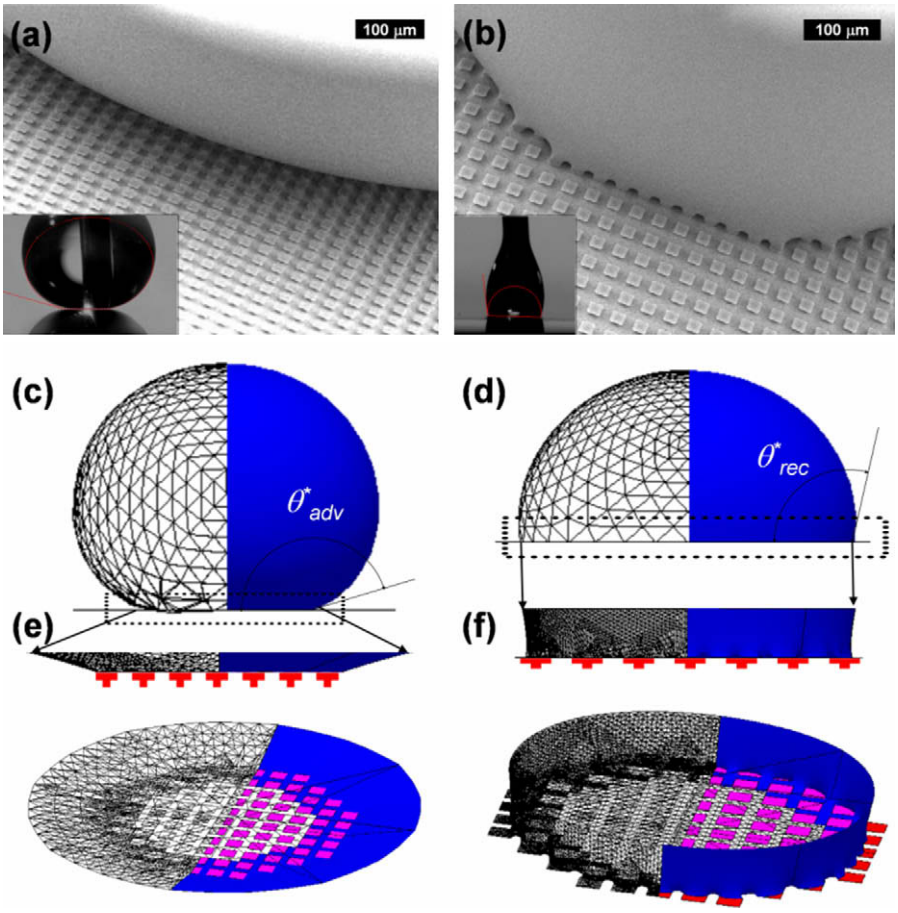

Fig. 3. Details of the advancing and receding TCL for a PDMS droplet on a discrete hoodoo surface. (a) Details of the TCL for an advancing droplet of PDMS on a discrete hoodoo surface ($\phi_s = 0.44$). The inset shows the apparent advancing angle for a droplet of decane ($\theta^*_{adv} = 164^\circ$) on this surface. (b) The details of the TCL for a receding droplet of PDMS on the same discrete hoodoo surface. The inset shows the apparent receding angle for a droplet of decane ($\theta^*_{rec} = 100^\circ$). (c) An FEM numerical simulation of an advancing droplet of decane (droplet volume = 30 μl, assuming 9.8 m/s^2 gravitational acceleration) on a discrete hoodoo surface, having an apparent contact angle close to 180°. The droplet cannot advance on the surface unless the apparent contact angle reaches the exact value of 180°; however, the image is generated at an apparent contact angle of 170° for a better visualization of the droplet. (d) An FEM simulation of a receding droplet of decane on the discrete hoodoo surface. The TCL starts to detach from the inner edges of the hoodoos at the apparent receding contact angle of $\theta^*_{rec} = 99^\circ$. (e, f) Simulated details of the TCL for advancing and receding droplets of PDMS on the discrete hoodoo surfaces.

Table 1
The relation between the differential parameter ϕ_d and the global parameter ϕ_s for various micro-hoodoo surfaces developed in this work.

Hoodoo surface	Analogous natural surface	$\phi_{d,adv}$	$\phi_{d,rec}$
Stripe-shaped, along the stripes	Butterfly wings, rice leaves	ϕ_s	ϕ_s
Stripe-shaped, across the stripes		0	ϕ_s
Discrete hoodoos	Lotus leaves, rose petals	0	$\sqrt{\phi_s}$
Inverse hoodoo[a]		$1-\sqrt{1-\phi_s}$	$1-\sqrt{1-\phi_s}$
Concentric ring-shaped hoodoos[a]		0	0
Spiral hoodoo		ϕ_s	ϕ_s

[a] As explained in the main text, for a receding TCL on the inverse hoodoo surface or the ring-shaped hoodoo surface, the value θ_2 in Eq. (3b) becomes equal to 0°, instead of 180°.

To further explore the effect of texture topography, specifically the connectivity of texture, we fabricated a surface that is the inverse of a normal discrete hoodoo surface (Fig. 4). This surface traps discrete pockets of air with the solid–liquid interface forming a continuous patchwork grid. For the inverse hoodoo surface, the global areal solid fraction was fixed at the same value as the discrete hoodoo surface shown in Fig. 3, $r_\phi\phi_s = \phi_s = 0.44$. In Fig. 4a, the shape of the advancing TCL on the inverse hoodoo surface can be observed. On this surface, $\min \phi_d|_{-\lambda}^{\lambda} = 1-\sqrt{1-\phi_s} \approx 0.25$ and $\max \phi_d|_{-\lambda}^{\lambda} = 1$ (see Supplementary material). Substituting the former value in Eq. (3) yields $\theta^*_{adv} = 131°$, which matches well with the measured value of $\theta^*_{adv} = 135°$. However, using a value of $\phi_{d,rec} = \max \phi_d|_{-\lambda}^{\lambda} = 1$ yields a predicted value of $\theta^*_{rec} = 70°$, which is significantly larger than the measured receding contact angle of $\theta^*_{rec} = 28°$. This discrepancy between the predicted and measured apparent receding contact angles arises from the lack of connectivity between the air pockets on the inverse hoodoo surface. In contrast to the case of discrete hoodoos, the TCL cannot readily detach from each of these discontinuous air pockets (see Supplementary material). Instead, the receding TCL leaves a residual thin liquid film on top of the air pockets, thus the local equilibrium contact angle θ_2 on the discrete air pockets becomes zero. Hence $\cos\theta_1 < \cos\theta_2$ for the receding TCL on the inverse hoodoo surface, and the apparent contact angle in Eq. (2) becomes minimized when the ratio $r_\phi\phi_d/(1-\phi_d)$ reaches its *minimum*. Thus a value of $\phi_{d,rec} = \min \phi_d|_{-\lambda}^{\lambda}$ should be used in Eq. (3). Substituting for $\theta_2 = 0°$, $\theta_1 = \theta_E = 70°$, and $\phi_{d,rec} = 1-\sqrt{1-\phi_s} \approx 0.25$ for Eq. (3) yields an apparent receding contact angle of $\theta^*_{rec} = 34°$, which matches well with the measured value of $\theta^*_{rec} = 28°$.

It is clear from the comparison between the apparent contact angles obtained for striped, discrete, and inverse hoodoo surfaces, that the global fraction ϕ_s does not directly control the value of CAH or the 'stickiness' [24,42] of drops (i.e., $\Delta\theta^* \neq f(\phi_s)$). Instead, the CAH is a function of topography and connectivity [9] of the surface micro-texture. Hence the incorporation of the local differential parameter ϕ_d, which captures how the nature of the local texture *varies* as the contact line is advanced or retracted, is crucial for accurate prediction of apparent contact angles or CAH. Motivated by this more explicit understanding, we fabricated model hoodoo geometries that can enhance or suppress stickiness by promoting or suppressing CAH. Fig. 5a and b shows two such model geometries – concentric rings and an Archimedean spiral (which is expressed in polar coordinates (R, Θ) by the equation $R = P\Theta/2\pi$, In this case, $P = 40$ μm, is the pitch between the stripes). For both of these surfaces, the size of the decane drop is significantly greater than the details of the surface texture (the diameter of the TCL (≈1 mm) ≫ hoodoo pitch (≈40 μm)), so the CB relation predicts a single value of the apparent contact angle ($\theta^*_E = 114°$) based on the global fraction $\phi_s = 0.44$. However, for the surface composed of a series of concentric rings (Fig. 5a and c), $\phi_{d,adv} = 0$, $\theta_{2,adv} = 180°$, and $\phi_{d,rec} = 0$, $\theta_{2,rec} = 0°$ (as was the case for the inverse hoodoo grid pattern). This maximal deviation between the advancing and receding contact lines promotes an extremely large CAH. Using Eq. (3), we obtain $\theta^*_{adv} = 180°$ and $\theta^*_{rec} = 0°$ for a droplet of decane on the concentric ring-shaped hoodoo surface. These values match well with the measured values of $\theta^*_{adv} = 160°$ and $\theta^*_{rec} = 0°$ (see insets of Fig. 5a).

On the other hand for the spiral surface, as a differential volume δV is added to (or removed from) the drop, the TCL incrementally advances, or recedes, by moving along the spiral stripe of the solid substrate. Thus, we expect $\phi_{d,adv} = \phi_{d,rec} = \phi_s$ (Fig. 5b and d; also see Supplementary material for further details). Therefore, a continuously connected re-entrant surface geometry such as the spiral hoodoo should lead to significantly lower CAH. Indeed, the measured apparent advancing and receding contact angles with decane ($\theta^*_{adv} = 121°$, $\theta^*_{rec} = 102°$, see insets of Fig. 5b) support this expectation. This observed low CAH cannot be predicted using a linear fraction or a local solid fraction, because these values are essentially indeterminate for the spiral hoodoo texture. This observation again highlights the wide applicability of the differential areal solid fraction $r_\phi\phi_d$ in computing accurate values of the apparent contact angles based on the modified CB relation (Eq. (3)).

In Fig. 6a, the measured values of the apparent advancing and receding contact angles are presented as a function of the global areal fraction ϕ_s for the various micro-hoodoo surfaces fabricated in this work. The predictions from the unmodified CB relation (Eq. (1)) are also shown. On a very coarse level, the CB relationship

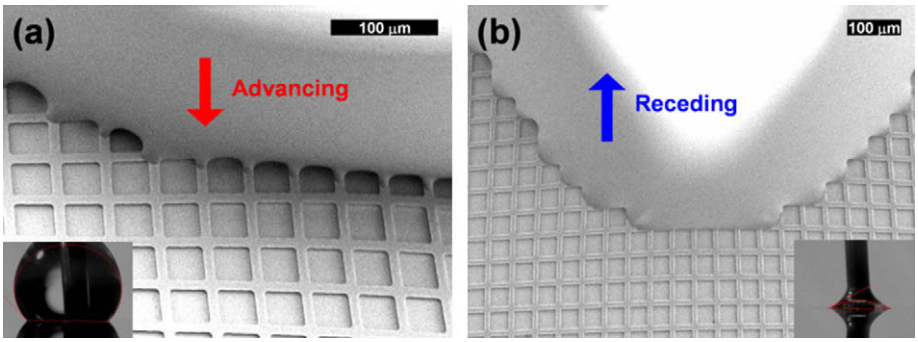

Fig. 4. Details of the advancing and receding TCL for a PDMS droplet on an inverse hoodoo surface. (a) The details of the TCL as the PDMS droplet advances on the inverse hoodoo surface ($\phi_s = 0.44$). The inset shows the apparent advancing angle for a droplet of decane ($\theta^*_{adv} = 135°$). (b) The details of the TCL as the PDMS droplet recedes on the same surface. The inset shows the apparent receding angle for a droplet of decane ($\theta^*_{rec} = 28°$).

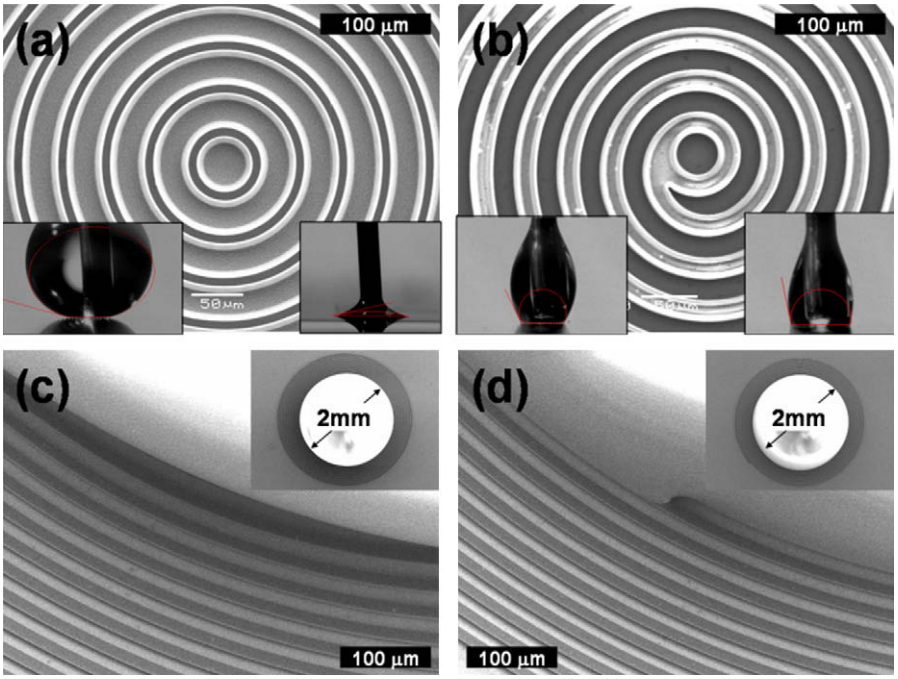

Fig. 5. Details of the advancing and receding TCL for PDMS droplets on a ring-shaped hoodoo surface and a spiral hoodoo surface. (a) Top view of a fabricated concentric ring-shaped hoodoo surface (ϕ_s = 0.44). The insets show the apparent advancing and receding angles for a droplet of decane ($\theta^*_{adv} = 160^\circ, \theta^*_{rec} \approx 0^\circ$). (b) Top view of a fabricated Archimedean spiral hoodoo surface (ϕ_s = 0.44). The insets show the apparent advancing and receding angles for a droplet of decane ($\theta^*_{adv} = 121^\circ, \theta^*_{rec} = 102^\circ$). (c) The details of the TCL for a droplet of PDMS (see inset) on a ring-shaped hoodoo surface. (d) The details of the TCL for a droplet of PDMS (see inset) on a spiral hoodoo surface.

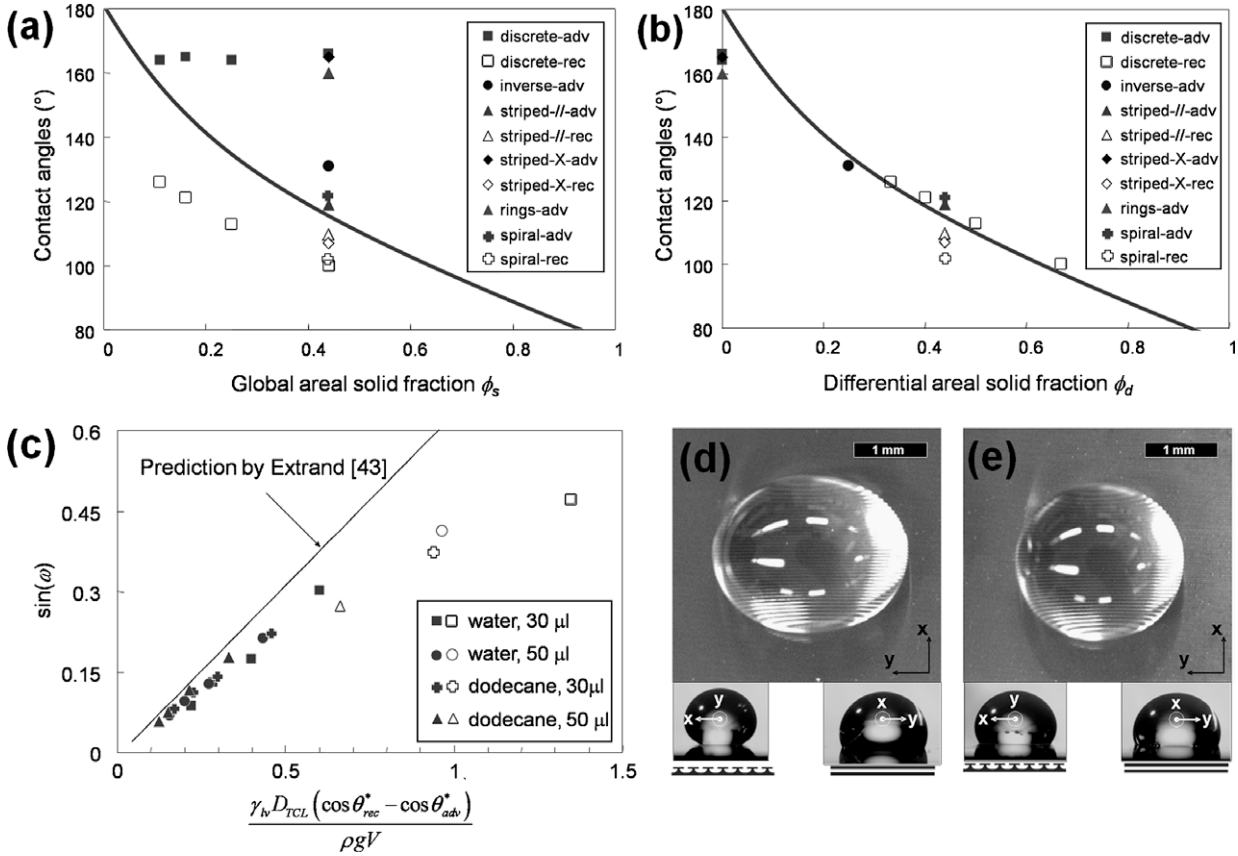

Fig. 6. (a) The measured apparent advancing and receding contact angles for decane droplets on the various hoodoo surfaces developed in this work, as a function of the global parameter ϕ_s. The apparent contact angle predictions from the classic CB relation (Eq. (1)) are also plotted as the solid line. (b) Same apparent contact angles, plotted against the differential parameter ϕ_d. The predictions from the modified CB relation (Eq. (3)) are also plotted as the solid line. For both Fig. 6a and b, the apparent receding contact angles on the inverse and ring-shaped hoodoos are not included as the θ_2 values for these cases are different (θ_2 = 0°) than the θ_2 values for all the other cases considered here. (c) Measured roll-off angles on discrete (filled) and inverse (hollow) hoodoo surfaces, plotted against the predicted values from Eq. (5). (d) Top view of a droplet of decane, deposited on a stripe-textured hoodoo surface. Insets show side views of the droplet, viewed along the *y*-axis (left) and the *x*-axis (right). (e) Top view of the same droplet of decane after vibration. Insets show the side views of the droplet, viewed along the *y*-axis (left, $\theta^*_x = 121^\circ$) and the *x*-axis (right, $\theta^*_y = 112^\circ$).

does describe the general trend in terms of the variation of apparent contact angle with increasing areal fraction. However the relationship provides no information on the CAH; which depends intimately on the details of the surface texture. For certain textures, e.g., stripe-textured or spiral hoodoo surfaces, the CAH is small and the CB relationship predicts the values of the observed apparent contact angles for a composite interface, within reason. However, in a general sense, the discrepancy between the CB relationship and the experimental data is significant and a more sophisticated measure of the wetted surface fraction is needed. In comparison, Fig. 6b shows the same apparent contact angle data plotted as a function of the differential areal fraction ϕ_d. The predictions from the modified CB relation (Eq. (3)) are also shown. Clearly, by considering the differential areal fraction of the solid surface in the vicinity of the TCL as it advances or recedes, Eq. (3) makes it possible to predict the apparent advancing and receding contact angles on the wide range of model surface textures presently considered. Table 1 summarizes the connection between ϕ_d and ϕ_s for the various micro-hoodoo surfaces developed in this work. It should be noted that Table 1, in conjunction with Eqs. (3a) and (3b), enables one to correlate the measured contact angle hysteresis with the global solid fraction ϕ_s. For example, the equation for the contact angle hysteresis on isotropically textured discrete hoodoo surfaces can be written as $\cos\theta^*_{adv} - \cos\theta^*_{rec} = \sqrt{\phi_s}(\cos\theta_E - 1)$. The resulting curve qualitatively matches the result from Reyssat and Quéré [22] who suggested the contact angle hysteresis on a dilute array of posts would be proportional to $\phi_s \ln(1/\phi_s)$ based on analysis of the three-dimensional shape of the liquid–air interface near the TCL.

As mentioned previously, the CB relation is unable to predict roll-off angles for a given contacting liquid on a textured substrate because the roll-off angle is strongly affected by the contact angle hysteresis. The roll-off angle ω is determined by a force balance between the gravitational body force acting on the drop and the resistance from the CAH along the perimeter [20]. Extrand and Gent developed a relation [43] to predict the roll-off angle ω without actually measuring the width of the droplet, which was needed by the previous models of Kawasaki [44] or Furmidge [45]. The Extrand–Gent model can be written as:

$$\sin\omega = \frac{2\gamma_{lv} D_{TCL}\left(\cos\theta^*_{rec} - \cos\theta^*_{adv}\right)}{\pi\rho g V} \tag{4}$$

where ρ and γ_{lv} are the density and surface tension of the liquid, respectively, g is the acceleration due to gravity, V is the volume of the droplet, and D_{TCL} is the average diameter of the TCL. The pre-factor $2/\pi$ arises because the shape of the droplet deviates from an ideal spherical cap due to the variation of the contact angle along the circumference of the droplet [43,46]. Clearly, it is necessary to be able to accurately determine θ^*_{adv} and θ^*_{rec} in order to predict the roll-off angle.

Combining Eq. (4) with the modified CB relation (Eq. (3)) for the apparent advancing and receding contact angles (see Supplementary material for details), we can predict the roll-off angle on a textured surface as:

$$\sin\omega \approx \frac{2\gamma_{lv} D_{TCL}\left((r_\phi\phi_{d,rec} - r_\phi\phi_{d,adv})\cos\theta_1 + (\phi_{d,rec} - \phi_{d,adv})\cos\theta_2\right)}{\pi\rho g V} \tag{5}$$

$$D_{TCL} \approx 2\cos(\bar{\theta}^* - \pi/2)\left(\frac{3V}{\pi(2 - 3\cos\bar{\theta}^* + \cos^3\bar{\theta}^*)}\right)^{1/3} \tag{5a}$$

where $\bar{\theta}^*$ is the average apparent contact angle ($\cos\bar{\theta}^* = (\cos\theta^*_{adv} + \cos\theta^*_{rec})/2$). Fig. 6c shows the measured roll-off angles of water (γ_{lv} = 72.1 mN/m, θ_E = 120°) and dodecane (γ_{lv} = 25.3 mN/m, θ_E = 73°) on the discrete and inverse micro-hoodoo surfaces, plotted against the prediction using Eq. (5). The strong correlation between the measured and predicted values demonstrates the utility of the modified CB relation in designing surfaces with small or large roll-off angles.

3.2. Reaching the equilibrium apparent contact angle through energetic perturbation

As first pointed out by Johnson and Dettre [5], a liquid droplet sitting on a composite interface reaches the true minimum in free energy when the apparent contact angle approaches θ^*_E. All other observed apparent contact angles, including the apparent advancing (θ^*_{adv}) and receding (θ^*_{rec}) contact angles, are metastable and correspond to higher free energy states [5,47]. The reason the equilibrium angle θ^*_E is rarely observed is because of the significant activation energy required to overcome the local energy barrier between each of the numerous metastable states in the energy landscape. Because of the robust nature of our composite solid–liquid–air interfaces, it is possible through careful external excitation to provide sufficient energy input to the system to allow the liquid droplet to overcome the energy barriers required to traverse multiple metastable states [5,48] without completely destroying the composite interface. In Fig. 6d a droplet of decane ($V \approx 50$ μl) on a stripe-textured hoodoo surface adopts an extremely anisotropic configuration. The insets in Fig. 6d show the shape of the decane droplet as viewed along the x and y directions with contact angles close to its advancing angles ($\theta^*_{adv,x} = 165°$ and $\theta^*_{adv,y} = 119°$). The hoodoo substrate, along with the droplet of decane, was then placed on a vibrating stage for a period of 2 min. The applied displacement profile was sinusoidal (frequency: 20 Hz, amplitude: 40 μm; maximum acceleration: 0.63 m/s^2). The volume of the droplet remains constant throughout the experiment, due to the low volatility of decane (vapor pressure: 187 Pa at 25 °C). Fig. 6e shows the shape of the decane droplet after the vibration process. It is clear that the droplet shape has become significantly more isotropic. The insets in Fig. 6e show the shape of the droplet as viewed along the x and y directions. The test was repeated nine additional times and the measured apparent contact angles ($\theta^*_x = 119 \pm 3°$ and $\theta^*_y = 113 \pm 2$) always matched more closely with the prediction for the apparent equilibrium contact angle ($\theta^*_E = 114°$), obtained from the classic CB relation. This result clearly demonstrates the ability of the classic CB relation to predict the equilibrium apparent contact angle; this ability was questioned by Gao and McCarthy very recently [49].

4. Conclusions

In conclusion, we have provided a unifying framework to reconcile the multiple scientific opinions in the literature regarding the validity, as well as the utility, of the CB relationship in estimating the apparent contact angles for a non-wetting drop forming a solid–liquid–air composite interface on a textured surface. In addition, by fabricating a range of robust oleophobic micro-hoodoo surfaces, we successfully imaged the local details of the TCL on a wide range of model surface topographies. Our experimental studies of both the local distortion of the TCL at the micron scale, as well as the measurement of the apparent contact angles at the macroscopic scale, clearly illustrates that the distortion of the TCL *per se* is not the key factor that leads to differences between the CB prediction and the measured values of the apparent advancing or receding contact angles. Instead, we show that the differential areal fraction of solid substrate which the TCL encounters as it is displaced across the surface is the most important factor in determining the apparent advancing and receding contact angles. This additional knowledge is embodied in the local differential

parameter ϕ_d. Using this insight, a modified CB relation is proposed that more accurately predicts the apparent advancing and receding contact angles, based on the details of the local surface texture in the proximity of the TCL. The validity of the modified CB model is demonstrated in Fig. 6b, which shows the close agreement between the prediction of this modified CB model and the measured contact angles on a range of hoodoo topographies. The equilibrium contact angle predicted by the classical CB relation can be recovered by 'relaxing' anisotropic advancing or receding pinned states using mechanical vibration. The local texture parameter ϕ_d can also be used to predict the roll-off angle ω for a given contacting liquid on a textured surface. This understanding allows us to design model 'sticky' or 'non-sticky' surfaces that can significantly enhance or suppress CAH and correspondingly increase or decrease measured roll-off angles.

Role of the funding source

The Air Force Research Laboratories contributed to this research by supplying the fluoroPOSS coating material and taking part in interpreting the data and writing the article.

Acknowledgments

This research has been supported by the Air Force Research Laboratory (AFRL) under Contract No. FA9300-06 M-T015 and the Air Force Office of Scientific Research (AFOSR) under contract no. FA9550-07-1-0272 and LRIR-92PL0COR. We also thank Prof. M.F. Rubner and the Institute for Soldier Nanotechnologies (ISN) at MIT for the use of various lab facilities.

Appendix A. Supplementary material

Supplementary data associated with this article can be found, in the online version, at doi:10.1016/j.jcis.2009.07.027.

References

[1] T. Young, Philos. Trans. R. Soc. London 95 (1805) 65.
[2] A.B.D. Cassie, S. Baxter, Trans. Faraday Soc. 40 (1944) 546–551.
[3] D. Quéré, M. Reyssat, Philos. Trans. R. Soc. A 366 (2008) 1539–1556.
[4] A. Marmur, Langmuir 19 (20) (2003) 8343–8348.
[5] R.E. Johnson, R.H. Dettre, Contact angle hysteresis, in: Contact Angle, Wettability and Adhesion, ACS Advances in Chemistry Series, vol. 43, American Chemical Society, Washington, DC, 1964, pp. 112–135.
[6] A. Tuteja, W. Choi, J.M. Mabry, G.H. McKinley, R.E. Cohen, Proc. Natl. Acad. Sci. 105 (47) (2008) 18200–18205.
[7] L. Gao, T.J. McCarthy, Langmuir 23 (7) (2007) 3762–3765.
[8] J. Drelich, J.D. Miller, A. Kumar, G.M. Whitesides, Colloids Surf., A 93 (1994) 1–13.
[9] W. Chen, A.Y. Fadeev, M.C. Hsieh, D. Oner, J. Youngblood, T.J. McCarthy, Langmuir 15 (10) (1999) 3395–3399.
[10] C.W. Extrand, Langmuir 18 (21) (2002) 7991–7999.
[11] C.W. Extrand, Langmuir 19 (9) (2003) 3793–3796.
[12] N.A. Patankar, Langmuir 19 (4) (2003) 1249–1253.
[13] C. Dorrer, J. Ruhe, Langmuir 22 (18) (2006) 7652–7657.
[14] Y.M. Zheng, X.F. Gao, L. Jiang, Soft Matter 3 (2) (2007) 178–182.
[15] N. Anantharaju, M.V. Panchagnula, S. Vedantam, S. Neti, S. Tatic-Lucic, Langmuir 23 (23) (2007) 11673–11676.
[16] G. McHale, Langmuir 23 (15) (2007) 8200–8205.
[17] M.V. Panchagnula, S. Vedantam, Langmuir 23 (26) (2007) 13242.
[18] M. Nosonovsky, Langmuir 23 (19) (2007) 9919–9920.
[19] L. Gao, A.Y. Fadeev, T.J. McCarthy, MRS Bull. 33 (8) (2008) 747–751.
[20] D. Quéré, Rep. Prog. Phys. 68 (11) (2005) 2495–2532.
[21] E.B. Dussan, R.T.P. Chow, J. Fluid. Mech. 137 (1983) 1–29.
[22] M. Reyssat, D. Quéré, J. Phys. Chem. B 113 (12) (2009) 3906–3909.
[23] W. Barthlott, C. Neinhuis, Planta 202 (1) (1997) 1–8.
[24] L. Feng, Y.A. Zhang, J.M. Xi, Y. Zhu, N. Wang, F. Xia, L. Jiang, Langmuir 24 (8) (2008) 4114–4119.
[25] L. Gao, T.J. McCarthy, Langmuir 23 (26) (2007) 13243.
[26] Y. Li, W.P. Cai, B.Q. Cao, G.T. Duan, F.Q. Sun, C.C. Li, L.C. Jia, Nanotechnology 17 (1) (2006) 238–243.
[27] P.S. Swain, R. Lipowsky, Langmuir 14 (23) (1998) 6772–6780.
[28] D.C. Pease, J. Phys. Chem. 49 (2) (1945) 107.
[29] M.J. Hey, J.G. Kingston, Chem. Phys. Lett. 447 (1–3) (2007) 44–48.
[30] K.K.S. Lau, J. Bico, K.B.K. Teo, M. Chhowalla, G.A.J. Amaratunga, W.I. Milne, G.H. McKinley, K.K. Gleason, Nano. Lett. 3 (12) (2003) 1701–1705.
[31] M. Nosonovsky, B. Bhushan, Langmuir 24 (4) (2008) 1525–1533.
[32] D. Öner, T.J. McCarthy, Langmuir 16 (20) (2000) 7777–7782.
[33] A. Ahuja, J.A. Taylor, V. Lifton, A.A. Sidorenko, T.R. Salamon, E.J. Lobaton, P. Kolodner, T.N. Krupenkin, Langmuir 24 (1) (2008) 9–14.
[34] A. Tuteja, W. Choi, M.L. Ma, J.M. Mabry, S.A. Mazzella, G.C. Rutledge, G.H. McKinley, R.E. Cohen, Science 318 (2007) 1618–1622.
[35] A. Tuteja, W. Choi, G.H. McKinley, R.E. Cohen, M.F. Rubner, MRS Bull. 33 (8) (2008) 752–758.
[36] W. Choi, A. Tuteja, S.S. Chhatre, J.M. Mabry, R.E. Cohen, G.H. McKinley, Adv. Mater. 21 (21) (2009) 2190–2195.
[37] W.A. Zisman, Relation of the equilibrium contact angle to liquid and solid construction, in: Contact Angle, Wettability and Adhesion, ACS Advances in Chemistry Series, vol. 43, American Chemical Society, Washington, DC, 1964, pp. 1–51.
[38] Z. Yoshimitsu, A. Nakajima, T. Watanabe, K. Hashimoto, Langmuir 18 (15) (2002) 5818–5822.
[39] Y. Chen, B. He, J.H. Lee, N.A. Patankar, J. Colloid Interface Sci. 281 (2) (2005) 458–464.
[40] L. Feng, S.H. Li, Y.S. Li, H.J. Li, L.J. Zhang, J. Zhai, Y.L. Song, B.Q. Liu, L. Jiang, D.B. Zhu, Adv. Mater. 14 (24) (2002) 1857–1860.
[41] K.A. Brakke, Philos. Trans. R. Soc. London 354 (1996) 2143–2157.
[42] D. Quéré, Physica A 313 (1–2) (2002) 32–46.
[43] C.W. Extrand, A.N. Gent, J. Colloid Interface Sci. 138 (2) (1990) 431–442.
[44] K. Kawasaki, J. Colloid Sci. 15 (1960) 402.
[45] C.G.L. Furmidge, J. Colloid Sci. 17 (1962) 309.
[46] A.I. ElSherbini, A.M. Jacobi, J. Colloid Interface Sci. 273 (2) (2004) 556–565.
[47] A. Marmur, J. Colloid Interface Sci. 168 (1) (1994) 40–46.
[48] R.E. Johnson, R.H. Dettre, J. Phys. Chem. 68 (7) (1964) 1744–1750.
[49] L. Gao, T.J. McCarthy, Langmuir 25 (13) (2009) 7249–7255.